

Article

A New Cytotoxic Dimeric Sesquiterpene Isolated from *Inula racemosa* Hook. f. (Root): In Vitro and In Silico Analyses

Rama Tyagi¹, Perwez Alam^{2,*†}, Md. Tabish Rehman², Mohamed Fahad AlAjmi^{2,*}, Afzal Hussain², Saima Amin³, Mohd. Mujeeb⁴ and Showkat R. Mir^{1,*}

¹ Phyto-Pharmaceutical Research Lab., School of Pharmaceutical Education and Research, Jamia Hamdard, PO Hamdard Nagar, New Delhi 110062, India; tyagirama8@gmail.com

² Department of Pharmacognosy, College of Pharmacy, Riyadh 11451, Saudi Arabia; m.tabish.rehman@gmail.com (M.T.R.); afzal.hussain.amu@gmail.com (A.H.)

³ Department of Pharmaceutics, School of Pharmaceutical Education and Research, Jamia Hamdard, PO Hamdard Nagar, New Delhi 110062, India; samin@jamiyahamdard.ac.in

⁴ Department of Pharmacognosy and Phytochemistry, School of Pharmaceutical Education and Research, Jamia Hamdard, New Delhi 110062, India; mmujeeb@jamiyahamdard.ac.in

* Correspondence: aperwez@ksu.edu.sa (P.A.); alajmister@gmail.com (M.F.A.); showkatrmir@gmail.com (S.R.M.); Tel.: +966-551362901 (P.A.); +966-114677191 (M.F.A.); +91-9811385772 (S.R.M.)

† Author to be considered as co-first author.

Abstract: A new dimeric sesquiterpene named disesquicin (compound **1**) was isolated from *Inula racemosa* roots by normal-phase MPLC (Medium Pressure Liquid Chromatography), and its structure was established by using extensive spectral analysis. Compound **1**, when tested on different human cancer cell lines, showed marked cytotoxic activity (IC₅₀ (μg/mL): 5.99 (MDA-MB), 9.10 (HeLa), and 12.47 (A549)). Docking study revealed that it binds at the catalytic domain of PLK-1 and interacts with catalytic site residues Leu59, Gly60, Lys61, Gly62, Cys67, Ala80, Lys82, Leu130, Arg136, Ser137, Leu139, Glu140, Lys178, Gly180, Asn181, Phe183, and Asp194. The binding of compound **1** to PLK-1 is spontaneous in nature as evident by a free energy of -8.930 kcal mol⁻¹, corresponding to a binding affinity of 3.54×10^6 M⁻¹. Results showed that compound **1** exhibited cytotoxic potential that was further confirmed by in vivo investigations.

Keywords: *Inula racemosa*; dimeric sesquiterpene; disesquicin; cytotoxicity; molecular docking; simulation



Citation: Tyagi, R.; Alam, P.; Rehman, M.T.; AlAjmi, M.F.; Hussain, A.; Amin, S.; Mujeeb, M.; Mir, S.R. A New Cytotoxic Dimeric Sesquiterpene Isolated from *Inula racemosa* Hook. f. (Root): In Vitro and In Silico Analyses. *Separations* **2021**, *8*, 2. <https://doi.org/10.3390/separations8010002>

Received: 18 November 2020

Accepted: 25 December 2020

Published: 29 December 2020

Publisher's Note: MDPI stays neutral with regard to jurisdictional claims in published maps and institutional affiliations.



Copyright: © 2020 by the authors. Licensee MDPI, Basel, Switzerland. This article is an open access article distributed under the terms and conditions of the Creative Commons Attribution (CC BY) license (<https://creativecommons.org/licenses/by/4.0/>).

1. Introduction

Cancer is one of the most deplorable diseases and a prevalent cause of worldwide death. According to the World Health Organization (WHO), nearly 9.5 million people died in 2018 due to cancer (<http://www.who.int/mediacentre/factsheets/fs297/en/>), and the main reason for death is the reappearance of treatment-resistant cancer cells in the infected area [1]. The widely available cancer treatment choices are surgery, chemotherapy and radiation therapy, which make patients' lives miserable due to their severe side effects. Polo-like kinases (PLK) belong to Ser/Thr kinase protein family, which tightly regulates the cell cycle and other cell processes. Among PLKs, PLK-1 is the most exclusively studied enzyme as it plays a significant role in cell cycle regulation and other cellular processes such as replication, transcription, translation, p53 regulation, dynamics of microtubules, recovery of different checkpoints, cell motility, etc. [2]. It has been reported that PLK-1 is overexpressed in many cancer cells such as breast cancer, ovarian cancer, skin cancer, etc. [3–5]. An analysis of the PLK-1 structure revealed two major druggable sites, namely (i) kinase domain harboring ATP binding site and (ii) polo-box domain. Previous studies have established that the ATP binding site in the kinase domain is the most preferred site for drug-designing. Since not many PLK-1 inhibitors are available in the market, there is a need to identify novel inhibitors, mostly from natural sources. The bioactive compounds from plants are preferred over synthetic drugs owing to

their lower side effects. Indeed, 50–60% of presently available anticancer drugs in the market (like taxol, vincristine, vinblastine etc.) are derived from natural product scaffold [6].

Inula racemosa Hook.f. (Asteraceae) grown extensively in China, Nepal, and in major parts of India has been used by mankind since ancient times to treat cancer, cardiovascular, and chronic dyspepsia [7]. *I. racemosa* has been reported to possess antiapoptotic property [8] and reportedly contains phytoconstituents like sesquiterpenoids and sesquiterpene lactones [9]. In this study, we report for the first time the isolation of a new dimeric sesquiterpene (Compound 1) from the roots of *I. racemosa*. Compound 1 was explored for its cytotoxic potential against different cancer cell lines such as HeLa (cervical), MDA-MB231 (breast), and A549 (lung) by MTT assay, and the in vitro results were validated by molecular docking and molecular dynamics simulation.

2. Materials and Methods

2.1. Plant Material

Inula racemosa roots were purchased from Universal Biotech (Gali Chashreen, Farash Khana, Chandni Chowk, India). A voucher specimen (PRL/2017/21) was stored in Phytochemistry Research Lab, Pharmacognosy Department of Jamia Hamdard, and Delhi-110062 for future reference.

2.2. Instruments

ATI Mattson genesis series Fourier transform (FT-IR) infrared spectrophotometer (Midland, Canada) was used to record IR spectra. Hewlett Packard 8452A diode array spectrophotometer (Palo Alto, CA, USA) was used to obtain UV spectra. Bruker Avance DRX 500 MHz and 125 MHz spectrometers (Billerica, MA, USA) were used to obtain 1D and 2D NMR spectra for ^1H and ^{13}C , respectively. Bruker Bioapex FT-MS was used to obtain the EI mass spectra.

2.3. Chemicals and Reagents

Silica gel (70–230 mesh) and LiChroprep RP-18 [40–63 μm ; octadecyl silica (ODS) gel] (Merck, Kenilworth, NJ, USA) were employed for column chromatography. The AR grade chemicals n-Hexane, ethyl acetate, chloroform, methanol, ethanol, sulphuric acid, and vanillin were procured from Faisal Zouman Al-Anazi Trading Est., Riyadh, Saudi Arabia. TLC was carried out on glass-backed silica gel F254 plate (Merck), and derivatization of plates was carried out by using *p*-anisaldehyde solution as a spray reagent.

2.4. Preparation of Methanolic Extract

Inula racemosa (roots) was cleaned, washed with water, and dried in an oven at 45 °C. The dried sample was pulverized to a coarse powder using a grinder. About 2700 g of powder was extracted in Soxhlet apparatus for 72 h with methanol (20 L). The extract was filtered and evaporated under reduced pressure at 65 °C in a rotary evaporator (Buchi India, Buchi Labortechnik AG, Flawil, Switzerland). A brownish viscous residue was obtained (762 g, 18.50% *w/w* yield).

2.5. Fractionation and Isolation of Phytoconstituents

The methanolic residue was suspended in water (1 L) and then fractionated with ethyl acetate. Ethyl acetate fraction further subjected to column chromatography. The ethyl acetate fraction was subjected to normal-phase MPLC. The preparative separation was carried out on an Easy Extract Purification System (Buchi Labortechnik, Flawil, Switzerland) consisting of two C-605 pump modules, a C-615 control unit, and a C-640 UV detector. The preparatory separation was carried out with a 70 × 460 mm plastic-glass column (Büchi, Switzerland) packed with silica gel Si60 (50–60 μm , Merck). Elution with hexane-ethyl acetate (80:20 *v/v*) resulted in the isolation of compound 1. Physical state: Cream coloured amorphous powder (0.52% yield), R_f : 0.83 (Toluene-chloroform-ethanol, 8:8:2), mp: 65–67 °C. UV λ_{max} (MeOH): 243, 270 nm; FTIR (KBr) ν_{max} : 3343, 2927, 2820, 1760, 1653,

1452, 1263, 1217, 1132, 771 cm^{-1} ; ^1H and ^{13}C NMR (CDCl_3): Table 1; +ve ES-MS m/z (*rel. int.*): 483 $[\text{M}+1]^+$ $\text{C}_{30}\text{H}_{43}\text{O}_5$ (2), 233 $[\text{C}_{15}\text{H}_{21}\text{O}_2]^+$ (48), 215 $[\text{C}_{15}\text{H}_{19}\text{O}]^+$ (80), 187 $[\text{C}_{14}\text{H}_{19}]^+$ (75).

Table 1. ^1H and ^{13}C NMR spectroscopic data of compound 1.

Position	δ_{H} (mult., J/Hz)	δ_{C} Type	Position	δ_{H} (mult., J/Hz)	δ_{C} Type
1	2.18, 2.16	41.8 CH_2	1'	1.31, 1.01	36.9 CH_2
2	1.25	27.5 CH_2	2'	1.23	16.8 CH_2
3	2.31 dt (9.2, 1.5)	32.8 CH_2	3'	2.10 dd (10.6, 1.9)	41.4 CH_2
4	2.43 m	37.7 CH	4'	-	149.1 C
5	-	149.0 C	5'	1.83 d (9.0)	46.2 CH
6	5.13 d (2.9)	118.8 CH	6'	1.50, 1.37	22.7 CH_2
7	3.55 m	39.5 CH	7'	2.95 m	40.6 CH
8	4.81 m	76.6 CH	8'	4.48 m	77.0 CH
9	1.72, 1.54	42.2 CH_2	9'	1.74, 1.57	42.7 CH_2
10	-	34.3 C	10'	-	34.3 C
11	-	139.9 C	11'	-	142.2 C
12	-	170.7 C	12'	-	170.8 C
13	6.18 s, 5.60 s	121.8 CH_2	13'	6.10 s, 5.57 s	120.2 CH_2
14	0.80 s	17.7 CH_3	14'	1.17 s	28.7 CH_3
15	1.08 d (5.4)	22.6 CH_3	15'	4.75 s, 4.42 s	106.7 CH_2

Data was recorded in CDCl_3 at 500 MHz for ^1H and at 125 MHz for ^{13}C NMR. The assignments were performed by DEPT, HMBC and HMQC experiments. Overlapped signals were included without the designated multiplicities.

2.6. Cytotoxicity Assay of Compound 1

2.6.1. Cell Culture and Treatments

The HeLa, MDA MB-231, and A549 cells were obtained from American Type Culture Collection (ATCC, Rockville, MD, USA). The cells were cultured in Dulbecco's modified Eagle's medium (DMEM, Sigma-Aldrich, St Louis, MO, USA) with 10% fetal bovine serum (FBS) and 1% penicillin/streptomycin in a completely humidified atmosphere with 95% air and 5% CO_2 at 37 °C. The exponentially growing cells were sub-cultured into 6-well or 96-well plates according to the experimental requirements. The viability of the cells was determined by the trypan blue test. The cells were counted using a cell counter (Bio Rad TC20 automated cell counter) and diluted in a medium at a density of 1×10^5 cells/mL to be used throughout the experiments. A stock solution of test compound 1 was prepared in DMSO (*w/v*) and was then diluted in cell culture medium (DMSO concentration decreased to less than 0.5% *w/v* to avoid its cytotoxic effect) [10] to obtain the desired concentrations for cell treatment.

2.6.2. Cytotoxicity Assay

A CellTite 96[®] non-radioactive cell proliferation assay kit (Promega, Madison, WI, USA) was used following the manufacturer's instructions to analyze the cytotoxic activity of compound 1 through MTT assay. Briefly, the HeLa, MDA MB-231, and A549 cells (1×10^4 cells/well) were grown overnight in 96-well flat-bottom cell culture plates and were then exposed for 24 h to six different concentrations of compound 1 (40, 20, 10, 5, 2.5 and 1 $\mu\text{g}/\text{mL}$). A negative control (untreated) was also maintained for comparison. After completing the desired treatment, 15 μL of MTT reagent, provided in the kit, was added to each well and further incubated for 3 h at 37 °C. Finally, the medium with MTT solution was removed, and 200 μL of solubilization solution was added to each well and further incubated for 30 min by occasional vortexing. The optical density (OD) of each well was measured at 550 nm using a Synergy microplate reader (BioTek, Winooski, VA, USA).

Results were generated from three independent experiments, and each experiment was performed in triplicate. The percentage of cytotoxicity compared to the untreated cells was estimated to determine the IC_{50} value (the concentration at which 50% cell proliferation is inhibited).

2.7. Molecular Docking and Molecular Dynamics Simulation

The interaction between compound **1** and different kinases (MEK1, ERK2, JNK, JAK, PKA, PLK-1, and CDK2) was elucidated by performing molecular docking using Glide-2018-4 (Schrodinger, LLC, NY, USA) in extra precision (XP) mode, as described previously [11]. Briefly, the ligand structure (compound **1**) was drawn in 2D sketcher, and the energy was minimized using OPLS3e forcefield. The 3D coordinates of kinases were downloaded from RCSB databank as MEK1 (PDB Id: 1S9J), ERK2 (PDB Id: 1wzy), JNK (PDB Id: 2P33), JAK (PDB Id: 4OLI), PKA (PDB Id: 6E99), PLK-1 (PDB Id: 2OWB), and CDK2 (PDB Id: 6GUE). The selection criteria for choosing the above mentioned crystal structures were (i) the structure should be solved by X-ray crystallography; NMR structures are not suitable for docking and simulation using Schrodinger suite, (ii) the resolution of structure should be $<2.5 \text{ \AA}$, (iii) the presence of a cognate ligand, which will help in the generation of a Grid file. Before molecular docking, the protein was preprocessed by adding missing hydrogen atoms, assigning bond orders, and deleting any hetero-atoms. Non-catalytic water molecules were also deleted. A fresh network of hydrogen bonds was created on the protein molecules after defining hydrogen atoms and energy of the whole system was minimized using OPLS3e force field. The dimensions of the Grid box and its location is given in Supplementary Table S1. The analysis and visualization of PLK-1-compound-1 interaction were performed in Maestro-2018-4 (Schrodinger, LLC, NY, USA). Binding affinity (K_d) of compound **1** towards proteins was determined from the docking free energy (ΔG) using the following relation [12,13].

$$\Delta G = -RT \ln K_d$$

where, R and T were Boltzmann gas constant ($=1.987 \text{ cal/mol/K}$) and temperature ($=298 \text{ K}$) respectively.

The dynamics and stability of the protein-ligand complex were estimated by performing molecular dynamics simulation for 50 ns using Desmond-2018-4 (Schrodinger, LLC, New York, NY, USA) as described previously [14,15]. Briefly, the protein-ligand complex was positioned in an orthorhombic-shaped simulation box, the boundaries of which were at least 10 \AA away from the protein-ligand complex. The simulation box was solvated using TIP3P explicit water model, and the system was neutralized with counterions. Further, 150 mM NaCl was added to simulate the physiological conditions. The OPLS3e force field was employed to pre-equilibrate the system by performing an iteration of 2000 steps with a convergence criterion of 1 kcal/mol/\AA . Finally, 50 ns simulation with NTP ensemble was performed at 300 K temperature and 1 bar pressure. The temperature and pressure of the system were maintained using Nose-Hoover Chain thermostat and a Matryna-Tobias-Klein barostate respectively [16,17]. During simulation, a 2 fs time step was set, and the energies/structures were recorded at every 10 ps in the trajectory.

2.8. Statistical Analysis

The statistical analysis of the triplicated samples (mean \pm SD) was carried out by one-way analysis of variance (ANOVA) followed by Dunnett's test.

3. Results and Discussion

3.1. Isolation of Compound **1**

Compound **1** was obtained as a cream colored amorphous powder from hexane-ethyl acetate (80:20 v/v) eluents. Its FTIR spectrum exhibited absorption bands for O-H stretching (3343 cm^{-1}), C=O stretching (1760 cm^{-1}), C=C stretching (1653 cm^{-1}) and C-H bending (1452 cm^{-1}). Based on $^{13}\text{C}/\text{DEPT}$ NMR and mass spectra, the molecular weight of

compound **1** was deduced to be 482 corresponding to the molecular formula $C_{30}H_{42}O_5$ of a sesquiterpene dimer (Figure 1). The formula indicated ten double-bond equivalents, four of which were adjusted in two bicyclic frameworks, four in vinylic linkages, and the remaining two in two carboxylic functionalities. Its +ve ES-MS displayed a fragment ion peak at m/z 233 [$C_{15}H_{21}O_2$]⁺ arising due to the fission of CH–O–CH linkage between two the sesquiterpenic units. The examination of 1D and 2D NMR spectra revealed thirty carbons consisting of eight quaternary, seven methine, twelve methylene, and three methyl carbons.

The ¹H NMR spectrum of compound **1** (Table 1) exhibited six one-proton singlets at δ 6.18 (H-13a), 5.60 (H-13b), 6.10 (H-13'a), 5.57 (H-13'b), 4.75 (H-15'a) and 4.42 (H-15'b) for the exocyclic vinylic protons. The ¹³C NMR spectrum displayed three pairs of downfield signals at δ 139.9 (C-11) and 121.8 (C-13), 142.2 (C-11') and 120.2 (C-13') and 149.1 (C-4') and 106.7 (C-15') that further supported the presence of three exocyclic vinylic linkages. The signals at δ 170.6 and 170.8 were assigned to the carboxylic carbons C-12 and C-12'. The cross peaks between the exocyclic vinylic protons (H₂-13/H₂-13') and the carboxylic carbons (C-12 and C-12', respectively) in the HMBC spectrum established the presence of two carboxyvinyl units in **1**. A doublet signal at δ 5.13 (1H, $J = 7.5$ Hz) was attributed to the cyclic vinylic proton H-6. The associated vinyl carbons resonated at δ 149.0 (C-5) and 118.8 (C-6). Two multiplets at δ 4.81 and 4.48, each integrating for one proton, were ascribed to the protons of the carbinol groups linking the two sesquiterpenic units. The corresponding carbon signals resonated at δ 76.6 (C-8) and 77.0 (C-8') in the ¹³C NMR spectrum. The HMBC spectrum displayed strong cross peaks between the carbinol protons H-8 and H-8' and C-6 and C-6', respectively. A three-proton doublet at δ 1.08 ($J = 5.4$ Hz) was attributed to the protons of the secondary methyl Me-15. Two singlets at δ 1.17 and 0.80, each integrating for three protons, were assigned to the protons of tertiary methyls Me-14' and Me-14, respectively. The NMR data of compound **1** was compared with other dimeric sesquiterpenes [18–21] and was found to differ significantly. Thus, the compound **1** was revealed to be a new heteromeric dimer of sesquiterpenes and was characterized as 8-(5,11(13)-eudesmadien-12-oic)-8-yl)oxy-4(15),11(13)-eudesmadien-8-yl-12-oic acid. The compound **1** was designated as Disesquicin.

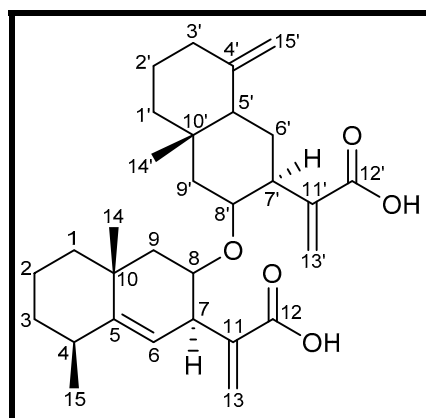


Figure 1. Chemical structure of compound **1**.

3.2. Cytotoxic Effect of Compound **1**

A variety of human cancer cell lines, i.e., cervical cancer (HeLa), breast cancer (MDA MB-231), and lung cancer (A549), were used for screening of the compound **1** by the standard method of MTT assay. A significant ($p < 0.05$) decrease in the cell viability was observed in all the cell line that was found to be concentration dependent (Figure 2). The cell proliferation was inhibited to 85%, 77% and 71% in MDA MB-231, HeLa, and A549 cells, respectively, at the highest concentration of 40 $\mu\text{g}/\text{mL}$. The IC_{50} ($\mu\text{g}/\text{mL}$) values estimated at 24 h post-treatment in these cells is 5.99 (MDA-MB cells), 9.10 (HeLa cells), and 12.47 (A549 cells). These data suggest that compound **1** exhibited higher cytotoxicity in breast cancer cells than the other cell lines.

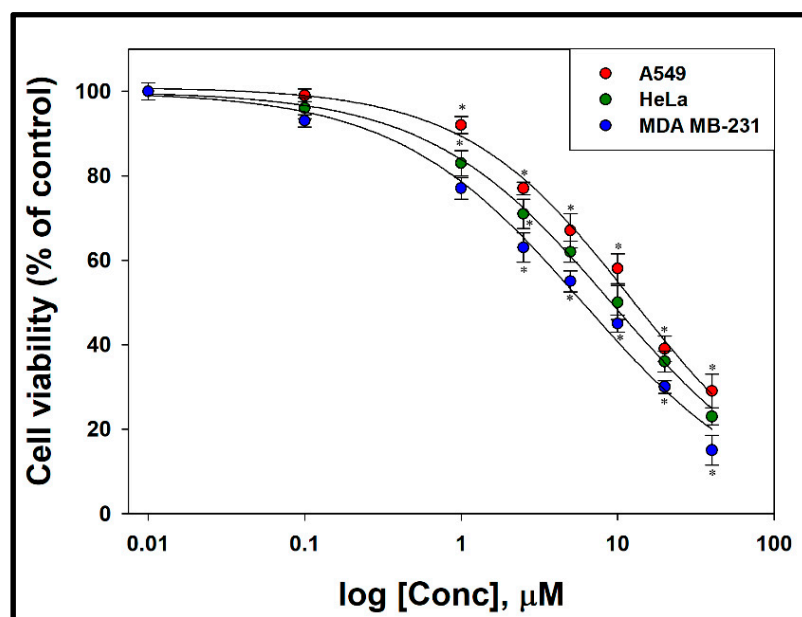


Figure 2. Cytotoxicity of compound 1 on MDA-MB cells, HeLa cells, and A549 cells treated in concentrations as indicated for 24 h and analyzed by MTT assay (All data are expressed as mean \pm SE from three independent experiments). * Significant ($p < 0.05$) compared with corresponding controls.

3.3. Molecular Docking Analysis

In order to elucidate the cytotoxic potential of compound 1, we performed molecular docking of compound 1 against different kinases. Supplementary Table S1 represents details such as target protein, their PDB Ids, cognate ligand, grid box and its location, and the binding energy of compound 1 and cognate ligand with the respective target. The binding energies of MEK1, ERK2, JNK, JAK, PKA, PLK-1, and CDK2 were -8.0 , -7.9 , -8.1 , -7.5 , -8.0 , -8.9 , and -8.1 kcal mol $^{-1}$, respectively (Supplementary Table S1). The complex between compound 1 and PLK-1 was chosen for further studies. PLK-1 (PDB Id: 2OWB) is solved at 2.10 Å resolution and harbors an ATP analog inhibitor (PHA680626). The chemical name of PHA680626 is 4-(4-methylpiperazin-1-yl)-*N*-[5-(2-thienylacetyl)-1,5-dihydropyrrolo [3,4-C]pyrazol-3-yl]benzamide. There were many crystal structures available for PLK-1, we chose 2OWB as the input structure for docking and simulation as it fulfilled the selection criteria of Schrodinger software (given in material and methods). Moreover, in our previous work, we used the same structure to identify Hesperidin as a potential inhibitor of PLK-1 [11]. It is worth mentioning that the reported crystal structure of PLK-1 harbors a T210V mutation. The residue T210 participates in the catalytic action and hence it was mutated to V210 during crystallography to avoid the hydrolysis of cognate ligand PHA680626.

The three-dimensional structure of PLK-1 can be categorized into a kinase domain, harboring ATP binding site, and a Polo-box domain. The ATP-binding site on the kinase domain is the most suitable site for an inhibitor to act on PLK-1. The X-ray crystal structure of PLK-1 reported by Kothe et al. [22] revealed that a non-hydrolyzable ATP analog PHA-680626 was bound at the active site of PLK-1. The cognate inhibitor (PHA-680626) interacts with Phe58, Lys82, Glu131, Arg134, and Asp194 [22]. Some hotspot residues of PLK-1 for binding an effective inhibitor were Cys67, Leu132, and Phe183. In the present study, the validity of molecular docking protocol was confirmed by re-docking the ligand present in the X-ray crystal structure of PLK-1, i.e., PHA680626, and compared the docking and crystal structure pose by calculating RMSD. We found that PHA680626 occupied a similar pose at the binding site of PLK-1 as occupied in the X-ray crystal structure. The RMSD between the docking pose and crystal structure pose was estimated to be 1.4373 Å (Supplementary Figure S7). Further, molecular docking between compound 1 and kinase domain PLK-1 has shown that the ligand occupied the ATP-binding site of PLK-1 (Figure 3). It formed two hydrogen bonds with Arg136 and nine hydrophobic interactions with Cys67, Ala80, Lys82, Leu130,

Leu139, and Phe183. Some other residues such as Leu59, Gly60, Lys61, Gly62, Ser137, Glu140, Lys178, Gly180, Asn181, and Asp194 also formed van der Waals' interaction with compound 1 (Table 2). It is interesting to note that compound 1 interacted with key and hotspot residues of PLK-1 such as Cys67, Lys82, Phe183, and Asp194, it could act as a potential inhibitor of PLK-1. The binding free energy and binding affinity of compound 1 towards PLK-1 were estimated to be $-8.930 \text{ kcal mol}^{-1}$ and $3.54 \times 10^6 \text{ M}^{-1}$, respectively.

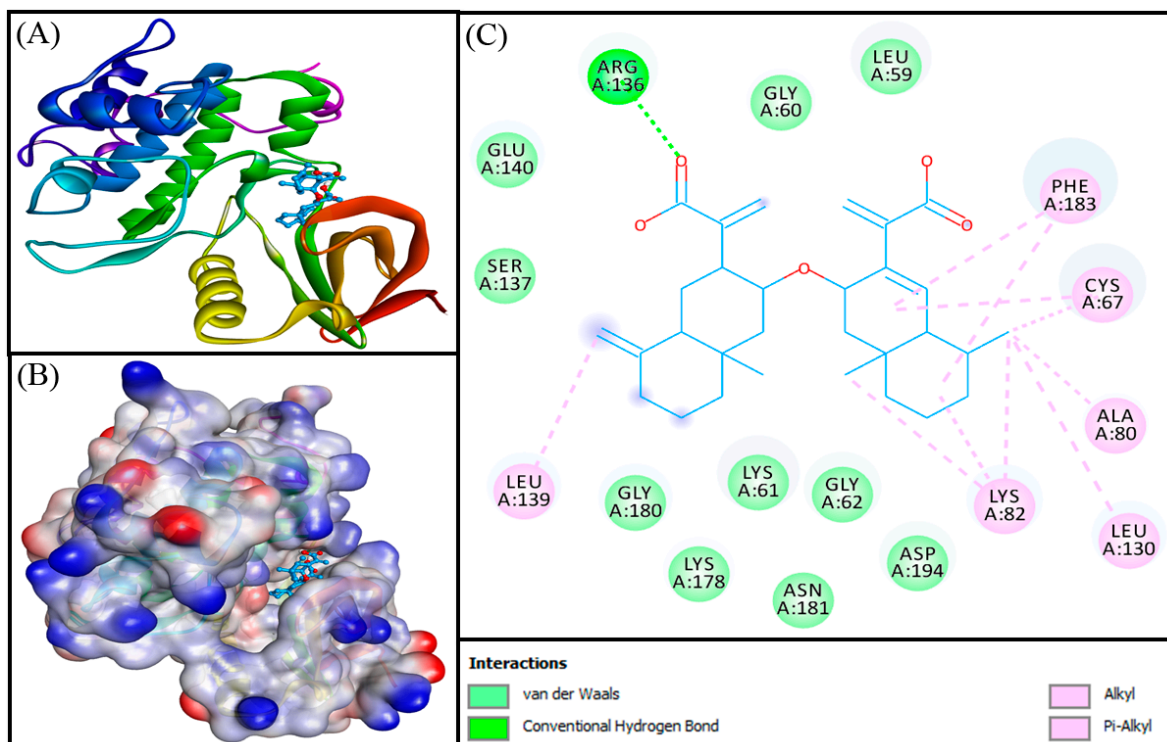


Figure 3. Molecular docking of compound 1 to the catalytic domain of Polo-like kinase 1 (PLK-1). (A) 2D representation of the binding of compound 1 at the ATP binding site of PLK-1, (B) binding of compound-1 at the ATP binding cavity of PLK-1, (C) molecular interaction between PLK-1 and compound 1.

For comparative analysis, the cognate ligand in the X-ray crystal structure of PLK-1, i.e., PHA-680626, was also docked to the active site of PLK-1 using the same procedure as adopted for PLK-1-compound 1 docking. The results revealed that PHA-680626 occupied a similar position at the active site of PLK-1 during molecular docking, as present in the X-ray structure. PHA-680626 formed two conventional and one carbon-hydrogen bond with Leu59, Lys82, and Cys133 of PLK-1; nine hydrophobic interactions with Leu59, Ala80, Val114 Arg136, and Phe183; and one electrostatic (Pi-Cation) interaction with Phe183, and one Pi-Sulfur bond with Cys133 (Figure 4). The residues forming van der Waals' interaction were Phe58, Gly62, Leu130, Glu131, Leu132, Arg134, Asn181, Gly193, and Asp194. The binding free energy of PHA-680626 towards PLK-1 was $-10.000 \text{ kcal mol}^{-1}$, and the corresponding binding affinity is $2.16 \times 10^7 \text{ M}^{-1}$ (Table 2). A 10-folds higher affinity of PHA680626 towards PLK-1 than compound 1 might be due to the formation of an electrostatic interaction and a Pi-sulfur bond. It is worthy to note that the amino acid residues of PLK-1 commonly involved in making contacts with PHA-680626 and compound 1 were Leu59, Gly62, Ala80, Lys82, Leu130, Arg136, Asn181, Phe183, and Asp194.

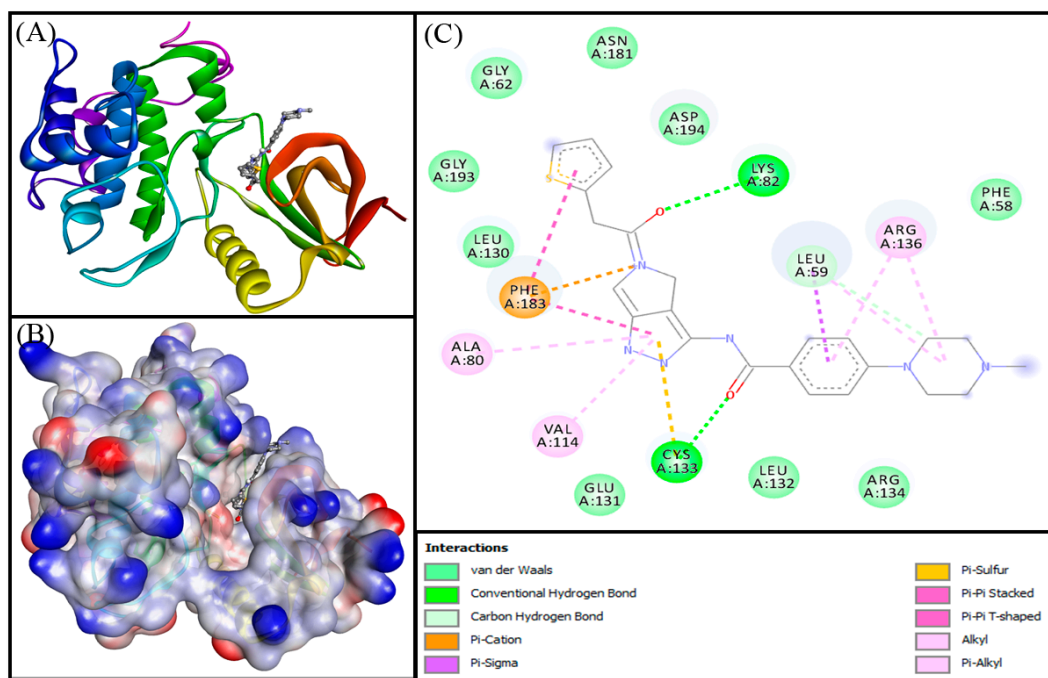


Figure 4. Molecular docking of PHA-680626 to the catalytic domain of Polo-like kinase 1 (PLK-1). (A) 2D representation of the binding of PHA-680626 (control ligand) at the ATP binding site of PLK-1, (B) binding of PHA-680626 (control ligand) at the ATP binding cavity of PLK-1, and (C) molecular interaction between PLK-1 and PHA-680626 (control ligand).

Table 2. Molecular docking parameters for compound 1-polo-like kinase (PLK-1) interactions.

Donor-Acceptor Pair	Distance (Å)	Type of Interaction	Docking Energy (kcal mol ⁻¹)	Docking Affinity, K _d (M ⁻¹)
Control (PHA-680626)				
LYS82:HZ3—Lig:O	2.7055	Conventional Hydrogen Bond	−10.000	2.16 × 10 ⁷
CYS133:HN—Lig:O	2.0328	Conventional Hydrogen Bond		
Lig:C—A:LEU59:O	3.3471	Carbon Hydrogen Bond		
Lig:N—A:PHE183	4.6259	Electrostatic (Pi-Cation)		
LEU59:CD1—Lig	3.7176	Hydrophobic (Pi-Sigma)		
LEU59:CD2—Lig	3.6603	Hydrophobic (Pi-Sigma)		
CYS133:SG—Lig	4.9895	Pi-Sulfur bond		
Lig—A:PHE183	3.6552	Hydrophobic (Pi-Pi Stacked)		
Lig—A:PHE183	5.7048	Hydrophobic (Pi-Pi T-shaped)		
LEU59—Lig	4.8864	Hydrophobic (Alkyl)		
ARG136—Lig	5.2156	Hydrophobic (Alkyl)		
Lig—A:ALA80	4.552	Hydrophobic (Pi-Alkyl)		
Lig—A:VAL114	4.7727	Hydrophobic (Pi-Alkyl)		
Lig—A:ARG136	4.8572	Hydrophobic (Pi-Alkyl)		
Compound 1				
ARG136:HE—Lig:O	1.9478	Conventional Hydrogen Bond	−8.930	3.54 × 10 ⁶
ARG136:HH21—Lig:O	2.8755	Conventional Hydrogen Bond		
CYS67—Lig	4.4491	Hydrophobic (Alkyl)		
LYS82—Lig	5.0996	Hydrophobic (Alkyl)		
Lig:C—A:CYS67	4.0577	Hydrophobic (Alkyl)		
Lig:C—A:LYS82	4.5342	Hydrophobic (Alkyl)		
Lig:C—A:LEU130	4.5272	Hydrophobic (Alkyl)		
Lig:C—A:LYS82	4.4063	Hydrophobic (Alkyl)		
Lig:C—A:LEU139	5.0879	Hydrophobic (Alkyl)		
PHE183—Lig	4.8694	Hydrophobic (Pi-Alkyl)		
PHE183—Lig	5.0389	Hydrophobic (Pi-Alkyl)		

3.4. Molecular Dynamics Simulation Analysis

3.4.1. Analysis of RMSD and RMSF

The dynamic nature of interaction and the stability of PLK-1-compound **1** complex was assessed by carrying out molecular dynamics simulation under physiological conditions. We also performed molecular dynamics of PLK-1-PHA680626 complex for the comparative analysis. The PLK-1-compound **1** complex's initial frame was subjected to molecular dynamics for 50 ns, and the results are presented in Figure 5. The root mean square deviation (RMSD) of a protein measures its deviation from the initial structure and accounts for protein stability during the simulation. The RMSD of PLK-1 alone for the initial 20 ns fluctuated between 0.0–2.2 Å and remained constant for the later part of the simulation (Figure 5A). It indicated that the structure of PLK-1 was not changed significantly during the simulation. The RMSD of PLK-1-compound **1** complex was within 1.2–1.6 Å for the initial 15 ns; within 0.73–1.84 Å for 16–20 ns, and with 1.6–2.4 Å towards the end of the simulation. Similarly, the RMSD of PLK-1-PHA680626 complex was within 1.0–3.0 Å for the initial 15 ns and within 1.5–2.6 Å for 21–50 ns. It should be noted that none of the fluctuations in RMSD were more than the acceptable limit of 2.0 Å. Since, compound **1** and the positive control PHA680626 behaved similarly during the molecular dynamics simulation, we infer that compound **1** was bound tightly to PLK-1 and formed a stable complex.

Root mean square fluctuation (RMSF) of a protein gives an insight into the local conformational changes in the side chains of a protein during the simulation. RMSF of PLK-1 alone, PLK-1-PHA680626 and PLK-1-compound **1** complexes are given in Figure 5B. It is evident that the RMSF of PLK-1 and PLK-1 in complex with compound **1** coincided, assuring that the overall conformation of PLK-1 remained conserved. For comparison, the RMSF deviations of PLK-1 and PHA680626 complex is also shown. It is evident that the N- and C-terminal regions of PLK-1 fluctuated most as they are in an unbound form. Additionally, the total number of contacts formed by PLK-1 with compound **1** and PHA680626 was also enumerated (Figure 6). The total number of contacts, in the form of hydrogen bonding, hydrophobic interactions, electrostatic interactions and van der Waals' interactions, between PLK-1 and compound **1** was varying between 0–6, with an average of 3.5 contacts (Figure 6A). Similarly, the total number of contact between PLK-1 and PHA680626 was between 1–9 throughout the simulation, with an average of 4.5 contacts (Figure 6B). Overall, these results confirmed the formation of a stable complex between PLK-1 and compound **1**.

3.4.2. Analysis of Structural Changes

The interaction between a ligand and protein often leads to changes in protein's secondary structural elements (SSE). Thus, a check on SSE variation during simulation is critical to overview the establishment of a stable PLK-1-compound **1** complex (Figure 7). The variation in total SSE (α -helix + β -sheet) of PLK-1 bound with compound **1** during simulation is presented in Figure 7A. We found that the total SSE of PLK-1 in complex with compound **1** was 44 % comprising 27% α -helix and 17% β -sheets, and it remained constant throughout the simulation. Additionally, the contribution of different amino acid residues in the formation of α -helices (light brown color bar) and β -sheets (teal color bar) is shown in Figure 7B. Overall, the results confirmed that PLK-1 and compound **1** complex was stable.

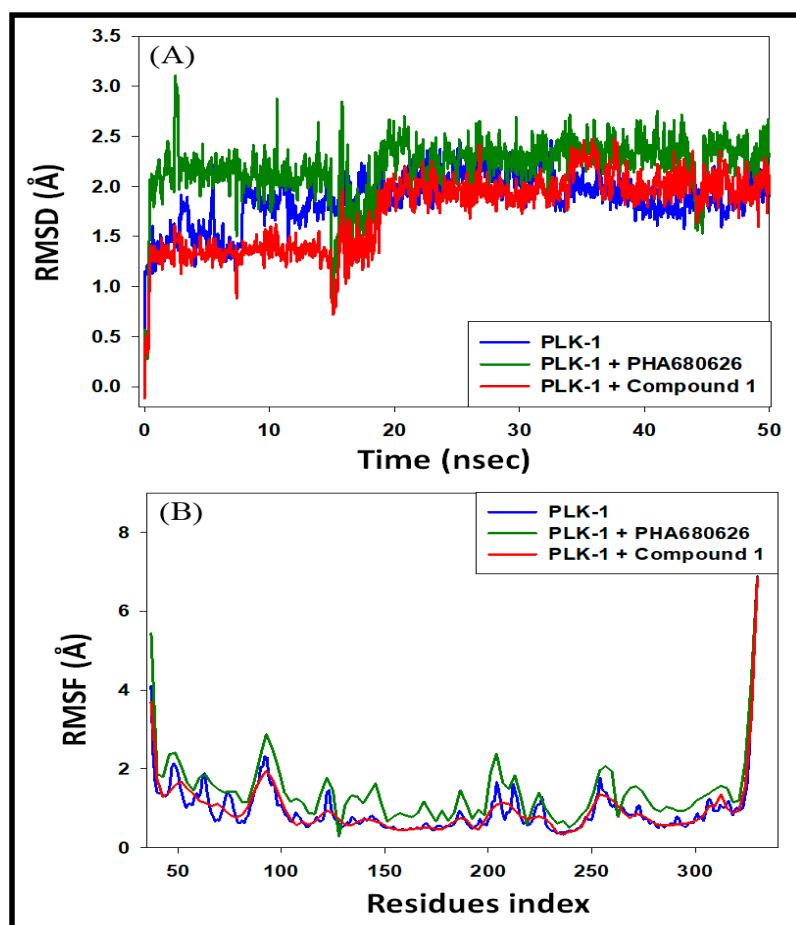


Figure 5. Molecular dynamics simulation of PLK-1 and compound 1 complex. (A) variation in root mean square deviation (RMSD). The curves in blue, green, and red show variations in PLK-1 alone, PLK-1-PHA680626 complex, and PLK-1-compound 1 complex. (B) variations in root mean square fluctuation (RMSF) as a function of simulation. The blue, green, and red curves show variation in RMSF of PLK-1, PLK-1-PHA680626 complex, and PLK-1-compound 1 complex, respectively.

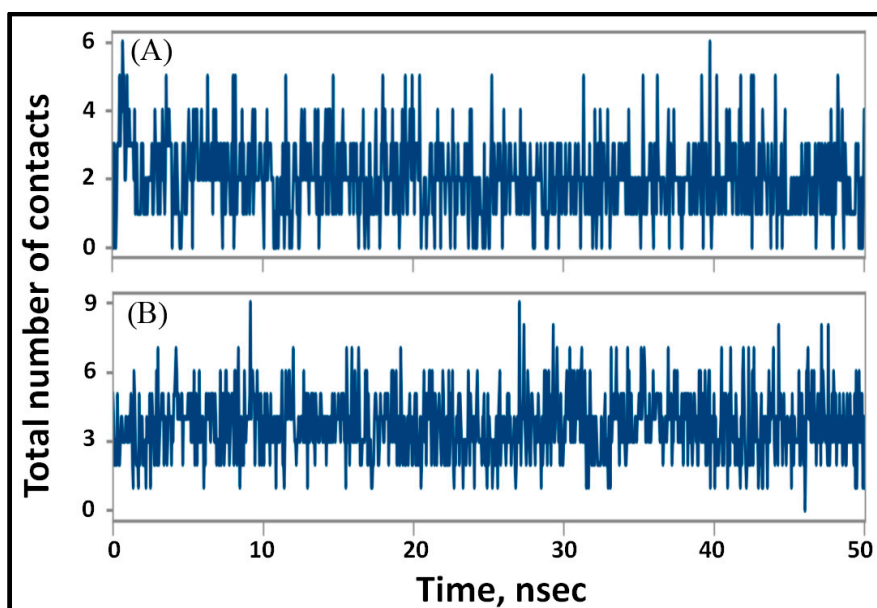


Figure 6. Variation in the total number of contacts formed between PLK-1 and (A) compound 1, and (B) PHA680626, as a function of simulation time.

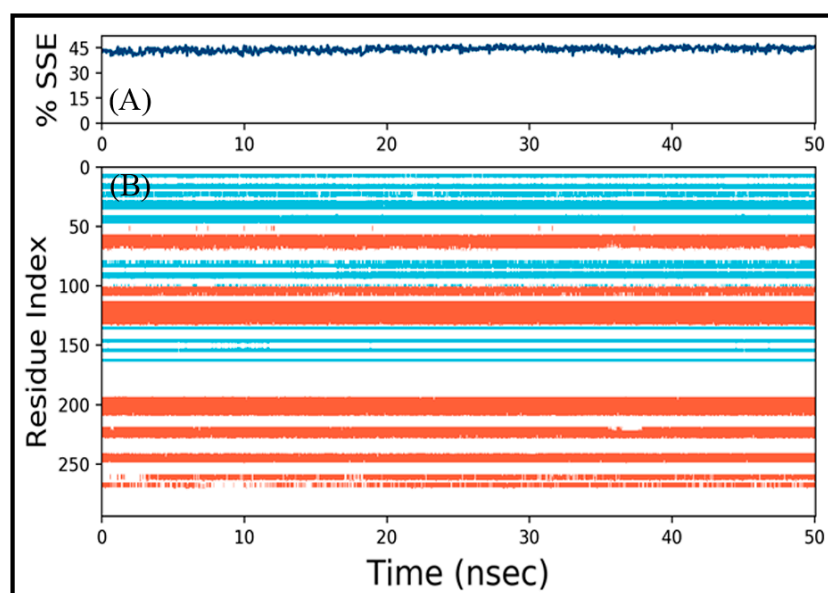


Figure 7. (A) Variation in secondary structure element (SSE) of PLK-1 during simulation, (B) participation of individual amino acid residues in contributing towards the formation of α -helices (light brown color bars) and β -sheets (teal color bars).

3.4.3. Analysis of Radius of Gyration (rGyr) and Surface Areas

The dependency of the radius of gyration (rGyr) and surface areas of a ligand on simulation time gives information about the ligand's behavior inside the binding pocket of the enzyme. The variation of rGyr of compound **1** with simulation time shows that it fluctuated for the initial 20 ns, and remained constant for the later part of the simulation. The range of rGyr for 21–50 ns was 4.8–5.2 Å, with an average value of 5.12 Å (Figure 8A). Similarly, the molecular surface area (MolSA), solvent accessible surface area (SASA), and polar surface area (PSA) of compound **1** varied significantly during 0–15 ns of simulation; however, they remained constant for 21–50 ns of simulation (Figure 8B–D). MolSA, SASA, and PSA values during 21–50 ns of the simulation were in the range of 420.0–435.9, 168.3–318.2, 130.9–146.2 Å² respectively. The average values of MolSA, SASA, and PSA during 21–50 ns simulation time were 424.6, 233.3, and 139.8 Å² respectively. For comparison, the variation in rGyr, MolSA, SASA, and PSA of PLK-1 alone and PLK-1-PHA680626 are also shown. In the case of PLK-1 alone, the values of rGyr, MolSA, and PSA did not change significantly over the simulation time. However, the SASA of PLK-1 without any ligand fluctuated for the initial 20 ns and then became stable. The average values of rGyr, MolSA, SASA and PSA of PLK-1 without any ligand in 21–50 ns range were estimated to be 5.03 Å, 424.2 Å², 192.8 Å² and 137.5 Å² respectively. Similarly, the values of rGyr, MolSA, and PSA of PLK-1-PHA680626 complex did not change significantly during simulation. However, the SASA of PLK-1-PHA680626 complex fluctuated for the initial 20 ns and then became stable. The average values of rGyr, MolSA, SASA and PSA of PLK-1-PHA680626 in 21–50 ns range were estimated to be 4.91 Å, 417.6 Å², 200.3 Å² and 134.2 Å² respectively. Since, the variations in rGyr, MolSA, SASA, and PSA of PLK-1-compound **1** complex were comparable to that of PLK-1 alone and PLK-1-PHA680626 complex, these results suggest that compound **1** remained inside the catalytic cavity of PLK-1 in a stable conformation.

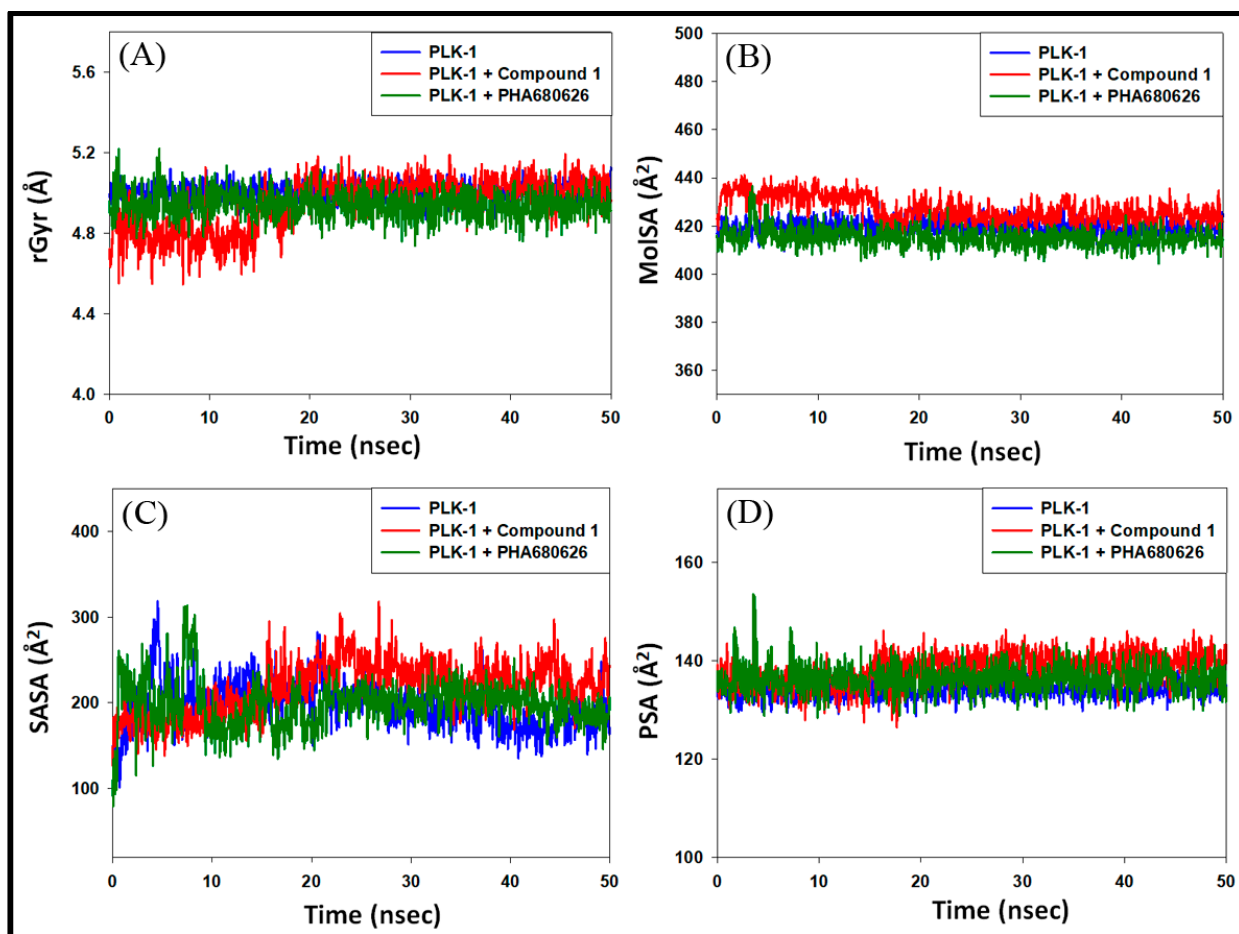


Figure 8. Dependency of (A) radius of gyration (rGyr), (B) molecular surface area (MolSA), (C) solvent accessible surface area, and (D) polar surface area of PLK-1, PLK-1-PHA680626 complex and PLK-1-compound 1 complex as a function of simulation.

4. Conclusions

This study reports the isolation of compound 1 (Disesquicin) for the first time from the roots of *Inula racemosa*. NMR and ES-MS spectra show that compound 1 belongs to the family of dimeric sesquiterpenes known for their anticancer and anti-inflammatory action. The anticancer activity of compound 1 by MTT assay confirmed its cytotoxic potential on three cell lines, i.e., HeLa (cervical), MDA-MB231 (breast), and A549 (lung). An insight into the cytotoxic potential of compound 1 reveals that it is more active against breast cancer cells. Here, we have employed an in silico approach to address our hypothesis that compound 1 could be a potential inhibitor of PLK-1, although there might be other possible targets also. An in silico molecular docking of compound 1 shows that it binds at the ATP binding cavity of PLK-1 and interacts with essential amino acid residues. Further, molecular dynamics simulation confirmed a stable PLK-1-compound 1 complex. We propose that compound 1 could serve as a scaffold to develop high affinity inhibitors of PLK-1 and need further biological studies for it to be a potential anticancer drug.

Supplementary Materials: The following are available online at <https://www.mdpi.com/2297-8739/8/1/2/s1>, Figure S1: ¹H NMR spectrum of compound 1 (Disesquicin). Figure S2: ¹³C NMR spectrum of compound 1 (Disesquicin). Figure S3: DEPT spectrum of compound 1 (Disesquicin). Figure S4: HMBC spectrum of compound 1 (Disesquicin). Figure S5: HMQC spectrum of compound 1 (Disesquicin). Figure S6: Mass spectrum of compound 1 (Disesquicin). Figure S7: Re-docking of PHA-680626 with PLK-1 and comparison of the docking pose (golden color) with the X-ray crystal

structure pose (teal color). The RMSD (root mean square deviation) between the two poses was 1.4373 Å. Table S1: Molecular docking parameters of compound 1 with different kinases.

Author Contributions: Conceptualization, S.R.M.; methodology, R.T.; validation, M.T.R. and A.H.; investigation, R.T., M.T.R. and P.A.; writing—original draft preparation, S.A., M.T.R. and P.A.; supervision, S.R.M. and M.M.; funding acquisition, M.F.A. All authors have read and agreed to the published version of the manuscript.

Funding: The authors would like to extend their sincere appreciation to the Deanship of Scientific Research at King Saud University for its funding of this research through the Research Group Project No. RGP-150.

Institutional Review Board Statement: Not applicable.

Informed Consent Statement: Not applicable.

Data Availability Statement: Data is contained within the article or supplementary material.

Conflicts of Interest: The authors declare no conflict of interest.

References

1. Sotillo, W.S.; Villagomez, R.; Smiljanic, S.; Huang, X.; Malakpour, A.; Kempengren, S.; Rodrigo, G.; Almanza, G.; Sterner, O.; Oredsson, S. Anti-cancer stem cell activity of a sesquiterpene lactone isolated from *Ambrosia arborescens* and of a synthetic derivative. *PLoS ONE* **2017**, *12*, e0184304. [[CrossRef](#)] [[PubMed](#)]
2. Lee, K.S.; Burke, T.R., Jr.; Park, J.E.; Bang, J.K.; Lee, E. Recent advances and new strategies in targeting PLK-1 for anticancer therapy. *Trends Pharm. Sci.* **2015**, *36*, 858–877. [[CrossRef](#)] [[PubMed](#)]
3. Takai, N.; Miyazaki, T.; Fujisawa, K.; Nasu, K.; Hamanaka, R.; Miyakawa, I. Expression of polo-like kinase in ovarian cancer is associated with histological grade and clinical stage. *Cancer Lett.* **2001**, *164*, 41–49. [[CrossRef](#)]
4. Weichert, W.; Kristiansen, G.; Winzer, K.-J.; Schmidt, M.; Gekeler, V.; Noske, A.; Müller, B.-M.; Niesporek, S.; Dietel, M.; Denkert, C. Polo-like kinase isoforms in breast cancer: Expression patterns and prognostic implications. *Virchows Arch.* **2005**, *446*, 442–450. [[CrossRef](#)]
5. Kneisel, L.; Strebhardt, K.; Bernd, A.; Wolter, M.; Binder, A.; Kaufmann, R. Expression of polo-like kinase (PLK1) in thin melanomas: A novel marker of metastatic disease. *J. Cutan. Pathol.* **2002**, *29*, 354–358. [[CrossRef](#)]
6. Gach, K.; Długosz, A.; Janecka, A. The role of oxidative stress in anticancer activity of sesquiterpene lactones. *Naunyn-Schmiedeberg's Arch. Pharmacol.* **2015**, *388*, 477–486. [[CrossRef](#)]
7. Firdous, Q.; Bhat, M.F.; Hussain, M.M. Ethnopharmacology, Phytochemistry and Biological activity of *Inula racemosa* hook. f: A review. *Int. J. Res. Ayurveda Pharm.* **2018**, *9*, 95–102. [[CrossRef](#)]
8. Arumugam, P.; Murugan, M. Antimutagenic and Antiapoptotic Effects of Aqueous Root Extract of *Inula racemosa* Hook. f. on 4-NQO-Induced Genetic Damage in Mice. *ISRN Pharmacol.* **2013**, *2013*, 1–5. [[CrossRef](#)]
9. Bohlmann, F.; Mahanta, P.K.; Jakupovic, J.; Rastogi, R.C.; Natu, A.A. New sesquiterpene lactones from *Inula* species. *Phytochemistry* **1978**, *17*, 1165–1172. [[CrossRef](#)]
10. Nguyen, S.T.; Nguyen, H.T.-L.; Truong, K.D. Comparative cytotoxic effects of methanol, ethanol and DMSO on human cancer cell lines. *Biomed. Res. Ther.* **2020**, *7*, 3855–3859. [[CrossRef](#)]
11. Alajmi, M.F.; Rehman, T.; Hussain, A.; Rather, G.M. Pharmacoinformatics approach for the identification of Polo-like kinase-1 inhibitors from natural sources as anti-cancer agents. *Int. J. Biol. Macromol.* **2018**, *116*, 173–181. [[CrossRef](#)] [[PubMed](#)]
12. Rehman, M.T.; Ahmed, S.; Khan, A.U. Interaction of meropenem with 'N' and 'B' isoforms of human serum albumin: A spectroscopic and molecular docking study. *J. Biomol. Struct. Dyn.* **2016**, *34*, 1849–1864. [[CrossRef](#)] [[PubMed](#)]
13. Braňka, A.C. Nosé-Hoover chain method for nonequilibrium molecular dynamics simulation. *Phys. Rev. E* **2000**, *61*, 4769–4773. [[CrossRef](#)] [[PubMed](#)]
14. Khan, M.S.; Bhat, S.A.; Rehman, T.; Hassan, I.; Tabrez, S.; Alajmi, M.F.; Hussain, A.; Husain, F.M.; Alamery, S.F. Rutin attenuates negatively charged surfactant (SDS)-induced lysozyme aggregation/amyloid formation and its cytotoxicity. *Int. J. Biol. Macromol.* **2018**, *120*, 45–58. [[CrossRef](#)]
15. AlShabib, N.A.; Khan, J.M.; Malik, A.; AlSenaidy, M.A.; Rehman, M.T.; AlAjmi, M.F.; AlSenaidy, A.M.; Husain, F.M.; Khan, R.H. Molecular insight into binding behavior of polyphenol (rutin) with beta lactoglobulin: Spectroscopic and computational studies. *J. Mol. Liq.* **2018**, *269*, 511–520. [[CrossRef](#)]
16. Rehman, T.; Shamsi, H.; Khan, A.U. Insight into the Binding Mechanism of Imipenem to Human Serum Albumin by Spectroscopic and Computational Approaches. *Mol. Pharm.* **2014**, *11*, 1785–1797. [[CrossRef](#)]
17. Martyna, G.J.; Tobias, D.J.; Klein, M.L. Constant pressure molecular dynamics algorithms. *J. Chem. Phys.* **1994**, *101*, 4177–4189. [[CrossRef](#)]
18. Qin, J.J.; Jin, H.Z.; Fu, J.J.; Hu, J.J.; Wang, Y.; Yan, S.K. Bioactive dimeric sesquiterpenes from *Inula japonica* thumb. *Bioorg. Med. Chem. Lett.* **2009**, *19*, 710–713. [[CrossRef](#)]

19. Qin, J.J.; Jin, H.Z.; Zhu, X.J.; Fu, J.J.; Hu, X.Z.; Liu, X.H.; Zhu, Y.; Yan, K.S.; Zhang, D.W. Neojaponicone A, a bioactive sesquiterpene lactone dimer with an unprecedented carbon skeleton from *Inula japonica*. *Chem. Commun.* **2011**, *47*, 1222–1224. [[CrossRef](#)]
20. Qin, J.-J.; Jin, H.; Zhu, J.; Fu, J.; Hu, X.; Liu, X.; Zhu, Y.; Yan, S.; Zhang, W.-D. Japonicones E–L, Dimeric Sesquiterpene Lactones from *Inula japonica* Thunb. *Planta Med.* **2009**, *76*, 278–283. [[CrossRef](#)]
21. Xu, X.Y.; Sun, P.; Guo, D.A.; Liu, X.; Liu, J.H.; Hu, L.H. Cytotoxic sesquiterpene lactone dimmers isolated from *Inula japonica*. *Fitoterapia* **2015**, *101*, 218–223. [[CrossRef](#)] [[PubMed](#)]
22. Kothe, M.; Kohls, D.; Low, S.; Coli, R.; Cheng, A.C.; Jacques, S.L.; Johnson, T.L.; Lewis, C.; Loh, C.; Nonomiya, J.; et al. Structure of the Catalytic Domain of Human Polo-like Kinase 1. *Biochemistry* **2007**, *46*, 5960–5971. [[CrossRef](#)] [[PubMed](#)]